

RESEARCH ARTICLE OPEN ACCESS

The Influence of Irradiation Wavelength on the Growth of Polymer Brushes by SI-PET-RAFT Polymerization

László Mérai¹ | Khrystyna Rymsha¹ | Jyoti Yadav¹ | Christian W. Pester² | Andreas Fery¹ | Quinn A. Besford¹ ¹Division Physical Chemistry and Physics of Polymers, Leibniz-Institut für Polymerforschung e.V., Dresden, Germany | ²Department of Materials Science and Engineering, University of Delaware, Newark, Delaware, USA**Correspondence:** Quinn A. Besford (besford@ipfdd.de)**Received:** 9 December 2024 | **Revised:** 12 January 2025 | **Accepted:** 13 January 2025**Funding:** The authors gratefully acknowledge the Deutsche Forschungsgemeinschaft (DFG) for funding project 496201730 ((BE 7737/2-1) (Q.A.B., K.R., L.M.)), and the Alexander von Humboldt Foundation (J.Y.).**Keywords:** photochemical action plots | photopolymerisation | polymer brushes | SI-PET-RAFT | wavelength-dependence

ABSTRACT

An effective method to produce well-defined polymer brushes with high spatial, temporal, and sequence control is to employ a photoredox catalyst in photo-mediated polymerization. Generally, the excitation wavelength is chosen as the absorption maximum of the photocatalyst, however, it is not clear if that corresponds to the best photochemical activity for producing polymer brushes. Herein, we systematically examine wavelength-by-wavelength resolved polymer brush growth using surface-initiated photoinduced electron transfer-reversible addition-fragmentation chain transfer polymerization (SI-PET-RAFT), of four monomer types. The absorption spectra of the water-soluble photocatalyst (ZnTPPS_4^{4-}) and the brush growth at each irradiation wavelength were examined as photochemical activity plots. Our results show a striking disparity between the absorbance of the photoredox catalyst and the maximum brush height. Moreover, the photochemical activity with wavelength was highly dependent on the nature of the monomer used. In addition to displaying a strong wavelength selectivity, a characteristic red-shift in the brush height relative to the lowest possible energy transition of the photocatalyst's absorbance spectrum was observed. We anticipate this work will better inform on wavelength choice for SI-PET-RAFT polymerization of polymer brushes.

1 | Introduction

Polymer brushes are a class of surface coating that offers an ability to control surface properties (fouling, wettability, etc.) [1–4], and in recent times, the emergence of exciting surface-based sensing technologies [5–8]. These systems consist of densely end-grafted polymer chains to an anchoring surface, such that the chains entropically “stretch” away from the surface. Methods to synthesize polymer brushes vary, though significant work has focused on reversible deactivation radical polymerization (RDRP) in a “grafting-from” approach, which produces well controlled thicknesses and grafting densities [9].

Prominent examples are photoinduced electron transfer radical polymerization (PET-RAFT) and photomediated atom transfer radical polymerization (photoATRP) [10]. In the case of the PET-RAFT polymerization, a photo-catalyst (PC) participates in photoinduced electron transfer to the chain transfer agent (CTA), generating a thiocarbonylthio anion [11]. The initiating step involves excitation of a PC by the energy absorbed at the irradiation with a specific wavelength; then, the excited-state PC interacts with the CTA through either an electron or an energy transfer process to fragment the transfer agent to give rise to the propagating radical. Generally, a transition metal catalyst or organic dye molecule represents a photocatalyst [12]. For

László Mérai, Khrystyna Rymsha, and Jyoti Yadav contributed equally.

This is for the special edition: 50 Years of Polymer Science at the Universität Bayreuth.

This is an open access article under the terms of the [Creative Commons Attribution](https://creativecommons.org/licenses/by/4.0/) License, which permits use, distribution and reproduction in any medium, provided the original work is properly cited.© 2025 The Author(s). *Journal of Polymer Science* published by Wiley Periodicals LLC.

successful photocontrolled RAFT polymerization, each step is selective toward reagents and reaction conditions and requires effective photolysis of the CTA (activation), selective insertion of the monomer into the CTA, and deactivation of the growing polymer chain end via a CTA [13]. Understanding the relationship between photo-excitation wavelength and the resulting brush properties is crucial toward developing the most efficient synthesis methods.

Several attempts at successful excitation of the PC with differing wavelength irradiations have been demonstrated in order to replace harmful UV-light initiating source with milder visible light sources. Shanmugam proposed to control polymerization rate through wavelength manipulation, and demonstrated the zinc tetraphenylporphyrin (ZnTPP) absorption profile over various visible wavelengths (460–655 nm). Kinetic experiments revealed that the polymerization rate was dependent on the light source, with fastest polymerization in yellow to slowest polymerisations in blue light [14]. The Pester group reported on the oxygen tolerance of SI-PET-RAFT in dimethylsulfoxide (DMSO) by using ZnTPP as a photocatalyst. In the study, the growth of *N,N*-dimethylacrylamide (DMA) brushes on 2-(Dodecylthiocarbonothioylthio)-2-methylpropionic acid (DDMAT)-functionalised silica substrates, as CTA, under yellow ($\lambda = 590$ nm) and blue ($\lambda = 405$ nm) irradiation [15]. The authors concluded that in case of the optimized conditions (increasing the amount of free DDMAT and using yellow light), the rate of polymerization could be decelerated while good control and high reproducibility of the thickness were maintained. This promoted utilization of ZnTPP in combination with DMSO for oxygen-tolerant SI-PET-RAFT polymerization under violet [16], green [17], or yellow light irradiation [18]. In an effort to promote green chemistry to the PET-RAFT process, aqueous photopolymerisation with oxygen tolerance in the presence of water-soluble zinc porphyrin photocatalyst (Zn(II) meso-tetra(4-sulfonatophenyl)porphyrin, ZnTPPS₄⁴⁻), with ascorbic acid as a singlet oxygen quencher, without prior deoxygenation emitting with red light ($\lambda_{\text{max}} = 635$ nm) was proposed [19]. Since then, aqueous SI-PET-RAFT photopolymerisation has been implemented [20]. It was proposed to use organo-dyes in the presence of tertiary amines as the metal-free photocatalytic system [21], among other eosin Y and fluorescein turned out to be the most efficient to activate polymerization and subsequently used under green and blue light irradiation [22, 23]. This method was employed for surface functionalization with polymer brush coatings and expanded to polymerization in continuous flow reactors [24], where oxygen tolerance and visible-light indication, aqueous media are highly advantageous for bioapplications [25]. Recently, Jazani et al., described oxygen-tolerant photo-RAFT polymerization in aqueous media in the presence of the sodium pyruvate (SP) and using 4-cyano-4-(phenylcarbonothioylthio)pentanoic acid (CPADB) as the CTA [10]. Depending on the irradiation wavelength, SP demonstrates different activity: at 370 nm SP decomposes to form CO₂ and radicals, initiating polymerization, under blue (450 nm) or green (525 nm) irradiation, SP enhanced the polymerization rate and decreased the induction period by interaction with excited state CPADB. In addition, observing RAFT polymerization in the absence of SP, with slower polymerization, was ascribed to weak absorption of light by the forbidden $n \rightarrow \pi^*$ transition of CPADB.

Recent studies by the Barner-Kowollik group have examined the correlation between the absorption of a chromophore and its photochemical reactivity. It was inferred that a molecule's absorption spectrum only informs about electronic excitations and refrains from providing information about the subsequent energy redistribution mechanisms [26]. The method of examining photochemical action plots (activity plotted against wavelength, with the absorption spectra), revealed an offset between the absorption and activity. Although this has been examined for basic photo-chemical reactions, and linear polymer synthesis, a detailed examination of photochemical action plots for brushes, via SI-PET-RAFT is missing, to our best knowledge.

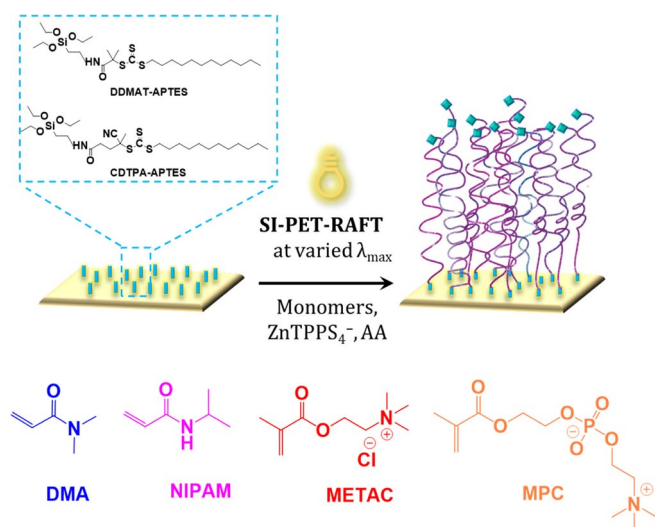
Herein, we examine the photochemical reactivity of ZnTPPS₄⁴⁻ for oxygen-tolerant aqueous SI-PET-RAFT polymerization, via the *R*-group approach, using the action plot methodology proposed by the Barner-Kowollik group [26]. Comparison of the PC absorbance spectrum with the wavelength-dependent polymerization of brushes, employing LEDs in the range 365–700 nm, allowed identification of the most efficient irradiation wavelengths with respect to brush height. Our method for comparing brush height against irradiation wavelength, allows for a straight forward comparison of photochemical activity for SI-PET-RAFT, without the need for quantifying polymer molecular weights, monomer conversions, and alike. This was done for a variety of monomers, including DMA, *N*-isopropylacrylamide (NIPAM), 2-methacryloyloxyethyl phosphorylcholine (MPC), and [2-(methacryloyloxy) ethyl]trimethylammoniumchlorid (METAC). Our results show unique offsets from the key absorption peaks, depending on the monomer type. We anticipate this will better inform the community on wavelength selection for SI-PET-RAFT for polymer brush synthesis.

2 | Results and Discussion

2.1 | Synthesis

Initially, both triethoxysilane-functionalised cyano-4-[(dodecylsulfanylthiocarbonyl)sulfanyl]pentanoic acid (CDTPA) and DDMAT derivatives were synthesized using a literature protocol (Scheme 1) [15], and were used as surface-tethered RAFT CTA initiators. A thin layer of these RAFT CTA (ca. 1.8 nm) was formed after silane-coupling to an activated R₃Si-OH wafer surface. For this study, we chose strongly hydrophilic DMA, weakly hydrophilic NIPAM, positively charged METAC, and zwitterionic MPC, as our monomers, to prove a diverse library. Brushes were assembled on substrates by depositing a pre-polymerization solution, comprising the monomer, an oxygen quencher (ascorbic acid), and the photocatalyst (ZnTPPS₄⁴⁻), on the wafers, and allowed to react under varied irradiation wavelengths using LED, with a constant light intensity of 1.82 mW cm⁻². After polymerization, the dry and wet brush thicknesses were quantified by spectroscopic ellipsometry, and water contact angles were measured.

The absorption intensity of the well-known meso-tetra(4-sulfonatophenyl) porphyrin (TPPS₄⁴⁻) molecule is mentioned in many studies, where the Soret region (around 430 nm) and partially in the Q region (around 650 nm) are attributed to transitions of molecular π , π^* orbitals of the porphyrin ring [27].



SCHEME 1 | Schematic of polymer brush synthesis using SI-PET-RAFT polymerization method. A solution of monomer, ascorbic acid, and photocatalyst (ZnTPPS_4^{4-}) is used to grow polymer brushes on substrates previously functionalised with RAFT CTAs (DDMAT or CDTPA) at varied wavelengths.

However, upon zinc ion incorporation, the intensity of Q band is decreased, while the Soret band exhibited a slight red shift from 400 to 405 nm, indicating improved structural symmetry and lowered energy gap in Zn metalloporphyrin photoredox catalyst [28]. Similar UV-Vis absorption maxima for ZnTPPS_4^{4-} in MilliQ were recorded at $\lambda_{\text{abs,max}} = 370, 405, 424$ (Soret band), 522, 554, 595 nm (Q bands) (Figure S1) [29]. Additionally, the UV-Vis absorption spectra of RAFT-CTAs used in this study was measured. Two distinct peaks at 320 nm (Soret) and 443 nm were observed for CDTPA and DDMAT CTAs corresponding to the $\pi-\pi^*$ and $n-\pi^*$.

2.2 | Tuning Light Wavelengths to Control the Polymer Brush Height

In the majority of earlier photoactivated polymerization methods, either the concentration of the catalyst or the intensity of the light was utilized to gradually control the polymerization rates, not often with different wavelengths, especially on ZnTPPS_4^{4-} photocatalyst [14, 30], to our best knowledge. Some previous studies suggested a mismatch between the highest possible efficiency of a photochemical process, that is, photo-reactivity, with that of the maximum absorption wavelength of a chromophore, and proved that the wavelength-dependent reactivity maximum is often red-shifted relative to the absorption maximum [31, 32]. This motivated our investigation of the conversion of a photochemical process (in terms of polymer brush height) at a range of monochromatic wavelengths to identify the most efficient irradiation condition. Therefore, in this study, we carried out polymerization tests under blue (365–480 nm), green (495–570), yellow (575–595 nm), orange (590–620 nm), and red LED light (620–700 nm) (Figure S2) for all chosen monomer systems. We point out that each of the LED systems have different emission breadths (Figure S2), where we focus on the peak of the emission profiles for comparing wavelength to brush growth. Furthermore, for systematic

comparisons we irradiate the samples with a constant flux in terms of energy per unit area (not number of photons).

Wafers were modified identically with DDMAT or CDTPA CTAs, where DMA and NIPAM were polymerized on DDMAT-modified wafers, whereas METAC and MPC were polymerized on CDTPA-modified surfaces. For polymerization, a constant irradiation of light at each monochromatic wavelength was used. Subsequently, brush growth as a function of irradiation wavelength was determined using an ellipsometer. Once the wavelength-dependent brush growth was defined, this was graphed jointly by overlaying the dry polymer brush height of each monomer with the UV-Vis absorption spectra of the photoredox catalyst, measured in MilliQ, resulting in the photocatalyst action plots (Figure 1). The absorption maximum of the photocatalyst was observed in the blue region at 425 nm. However, the action plot indicates a red-extended wavelength regime with the highest brush heights achieved at 617, 490, and 565 nm for pDMA, pMETAC, and pMPC, respectively. Similarly, for pNIPAM, a maximum brush height was observed at wavelength 405 nm which was significantly blue-shifted with respect to the 425 nm absorption maxima. Importantly, some previous studies have shown that CDTPA and DDMAT act as photoiniferters, therefore, undergo photolysis to generate radicals initiating RAFT polymerization without needing a photoredox catalyst in the presence of blue and green irradiation. For example, under blue irradiation at 365 nm, trithiocarbonate moiety displays living characteristics, but only low conversions were obtained under long irradiation times. While for visible light, the polymerization depended highly on the concentration of CTAs [33, 34]. The absorbance spectra for CDTPA and DDMAT are shown in Figure S3a, where we note there are no distinct peaks in brush height that correspond to the CTAs' absorbance profiles, meaning the CTAs should not be acting as photo-iniferters in our systems. This conclusion is further supported by control brush syntheses: without the application of photocatalyst, the achieved brush height was negligible even at lower wavelengths (<1.2 nm) (Figure S3b). Surprisingly, nearly all of the generated action plots show a marked mismatch between the photocatalyst absorption bands and the maximum brush height achieved, often finding the maximum reactivity in regions of very low absorptivity. We observed an approximate 20-nm red-shift in all action plots with respect to the lowest possible energy transition (Figure S4). We note that there appeared to be similarity between the same CTAs, and differences between DDMAT and CDTPA. For example, systems with DDMAT (NIPAM and DMA) exhibited minima in heights which were not present for CDTPA (METAC and MPC). This hints that the photochemical activation might be a function of both the CTA and the photocatalyst.

The brush heights of all the studied monomers were smaller in the irradiation-wavelengths ranging from 650 to 700 nm. Although the heights are lower in this range, it is nonetheless interesting to observe brush growth at such red-shifted wavelengths. Previous studies suggest no photolysis of DDMAT and CDTPA takes place in red light, indicating that self-initiation is not feasible at this wavelength range. Therefore, ruling out the possibility of their sole participation in initiating polymerization. To understand this in-depth, UV-Vis absorption spectra of ZnTPPS_4^{4-} with ascorbic acid and of the pre-polymerization

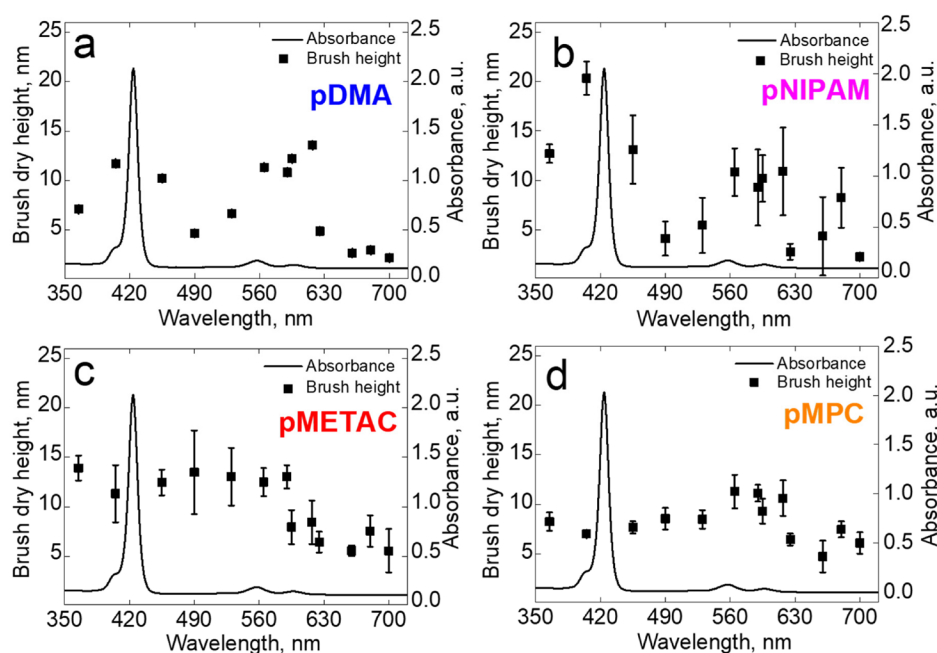


FIGURE 1 | Wavelength-dependent dry brush height using SI-PET-RAFT polymerization for (a) DMA, (b) NIPAM, (c) METAC, and (d) MPC systems after 10 min of constant flux of irradiation (except for METAC, 20 min) overlaid with the photocatalyst absorbance spectra. Each wavelength-resolved experiment was repeated in triplicates, the data point shows the average value and error bars indicate standard deviations. We note that the wavelength is given in terms of the peak of the emission spectra of the LED sources, which all have different breadths (Figure S2).

solution containing (ZnTPPS_4^{4-} , ascorbic acid, and monomer in the absence of RAFT agent) before and after irradiation were recorded. We noted that the absorption spectrum of pure ZnTPPS_4^{4-} did not have any peak at 650 nm (Figure S1), however, once ascorbic acid is added, it became visible (Figure S5). Notably, the presence of ascorbic acid not only aids in quenching singlet oxygen but also acts as a sacrificial electron donor to accelerate polymerization. The appearance of two additional peaks at 625 nm (only in case of pDMA and pNIPAM solutions) and the onset of 715 nm were noticed while one at 650 nm persisted (Figure S6). This could be associated with partial protonation of photoredox catalyst due to a negative pK_a shift [29, 35], and formation of J-aggregates [36], respectively. The reason to observe this significant difference in the absorption peak at 650 nm and probably an associated increased polymer brush height at 680 nm might be explained by the activation of the trithiocarbonate RAFT moiety on the substrates (which is absent during bulk photopolymerisation). Usually, upon irradiation, ZnTPPS_4^{4-} is reduced to $((\text{ZnTPPS}_4^{4-})^-)$ reduced porphyrin) form specifically activating the trithiocarbonate moiety of the CTA through an electron transfer that produces the RAFT radicals, leading to further polymerization in the presence of monomers [19, 37].

2.3 | Wavelength-Dependent Swelling Ratio

Evaluating the degree of swelling of a brush allows an estimation on the average hydrophilicity of the brush. Generally, in good solvents, tethered layers swell. The swelling behavior of polymer brushes was evaluated using the swelling ratio, which is the ratio of swollen brush thickness to the dry brush thickness. The thickness of the swollen layers is

governed by the balance between osmotic pressure and chain stretching. Figure 2 presents the ellipsometrically determined brush thickness and resultant swelling ratio as a function of irradiation-wavelength. We note that the degree of swelling depends highly on the grafting density. However, in our studies, since the RAFT-CTA-APTES modifications on all activated silica wafers were followed identically, and in one batch, the grafting density is assumed the same for each system. We note that we use the *R*-group approach for SI-PET-RAFT, meaning that the macromolecule never detaches from the surface [15]. The estimated swelling ratios for pDMA brushes (Figure 2a) were in the range of (5.7–10) implying a higher hydrophilicity [38]. In a similar way to pDMA brushes, pNIPAM also swelled in water however with lower swelling ratios and higher errors. These errors imply a higher chain dispersity in these brushes. Furthermore, RAFT CTA layers did not cause these greater chain dispersities; rather, their layer thickness was very uniform, measuring 1.4 ± 0.1 nm for DDMAT and 2.1 ± 0.1 nm for CDTPA. This inhomogeneity could arise from the use of mixed solvents during pNIPAM synthesis (i.e., due to the solubility of NIPAM). In addition, compared to pDMA brushes, the secondary amide of pNIPAM can result in strong interchain hydrogen bonding between the secondary amides and water molecules, which prevents swelling [38, 39]. Consequently, we can conclude that within the scope of our experiments (with the given monomers and SI-PET-RAFT polymerization), increased dry brush thickness errors result in even more pronounced wet brush error deviations. The swelling ratios for the pMETAC and pMPC brushes in Figure 2c,d had comparable trends, ranging from (2–7) to (4–8), respectively [40]. Interestingly, for all monomers, the patterns between the local minima in dry height nicely support the swelling ratio.

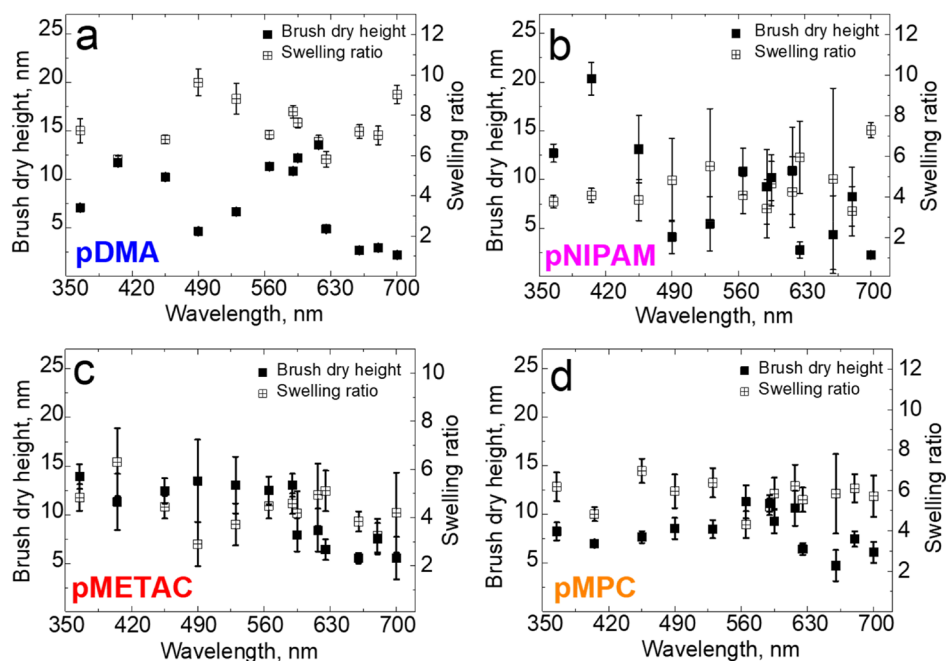


FIGURE 2 | Wavelength-dependent swelling ratios of (a) pDMA, (b) pNIPAM, (c) pMETAC, and (d) pMPC brushes after 10 min of irradiation (except for pMETAC, 20 min) overlaid with their dry heights. All measurements were carried out in triplicates and the error bars indicate the standard deviation of the data.

2.4 | Wettability

The polymer brush height and swelling are fundamental comparative descriptors to polymer brushes, however, further information on brush properties can be gleaned from wettability, which can also be indicative of brush height [41, 42], or dispersity [43, 44]. To assess how brush wettability was influenced by the height differences due to irradiation wavelengths, the advancing (ACA) and receding contact angles (RCA) against water during dynamic contact angle (DCA) measurements were recorded. The main advantage of DCA determinations over simpler static, sessile drop contact angle experiments is the better insight into the presence of possible surface inhomogeneities and swelling (liquid retention) phenomena through the comparison of contact angle hysteresis (CAH) values [45, 46], while the unwanted uncertainties of sessile drop measurements, such as errors from droplet spreading and evaporation can also be ruled out.

Initially, the functionalisation of the originally hydrophilic silica substrates ($ACA = 33.2^\circ \pm 0.1^\circ$, $RCA = 22.9^\circ \pm 0.1^\circ$) with both RAFT-CTAs rendered the surfaces more hydrophobic (DDMAT: $ACA = 69.6^\circ \pm 0.1^\circ$, $RCA = 52.9^\circ \pm 0.1^\circ$; CDTPA: $ACA = 99.3^\circ \pm 0.2^\circ$, $RCA = 74.6^\circ \pm 0.2^\circ$), likely due to their hydrophobic Z-groups (dodecyl-groups in the case of both DDMAT and CDTPA). Generally, grafting with polymer brushes rendered the surfaces more hydrophilic, which was found to be a function of both the polymer type and the brush height (Figure 3).

As Figure 4 shows, there are generally decreasing trends in DCA with increasing dry height (DCA vs. wet height is shown in Figure S7). This is in accordance with the hydrophilic nature of the monomers and with previous experimental observations on few nm thick polymer brushes with low substrate coverage

[42, 47]. While the majority of related literature examples show increasing contact angles on hydrophilic brushes of increasing height, this can clearly be attributed to the examined thicker (height is usually larger than 20 nm) brush regimes, and/or higher grafting densities [43, 48]. As examples of this, Yang et al., reported increasing static contact angles with the increasing height of poly(2-hydroxyethyl-methacrylate) brushes in the ~0–90 nm range, which they attributed to the hydroxyl group-mediated aggregation of polymer chains [49], while the similar, grafting density-dependent dynamic wetting behavior of zwitterionic polymer brushes was also reported [50].

Despite the direct effect of brush grafting density on wetting was not in the focus of this study, due to all substrates being functionalised with the surface initiator under the same conditions, the DCA were not affected by grafting density variation, and the decreasing tendencies with increasing height might have been allowed by grafting densities lower than those achieved in the cited references. Although, systematically examining their possible influence was not in the scope of this study, it is assumed, that the overall wettability in the few-nanometer height regime might also have been affected by the brush end-groups originated from the RAFT CTAs, since they might have higher relative effect on interfacial brush orientation.

The influence of height in the examined regime over wettability is also confirmed by the lack of obvious correlation between swelling ratios and CAHs (Figure S8), while unambiguous correlations between DCAs and swelling ratios could also not be observed (Figure S9). The pMETAC brushes grafted under $\lambda = 365$, 455, and 530 nm were superhydrophilic, having extremely low contact angles ($DCA < 1.8^\circ$), surpassing the limitations of the applied drop contour-fitting method, therefore all undeterminable ACA and RCA were denoted as 1.8° .

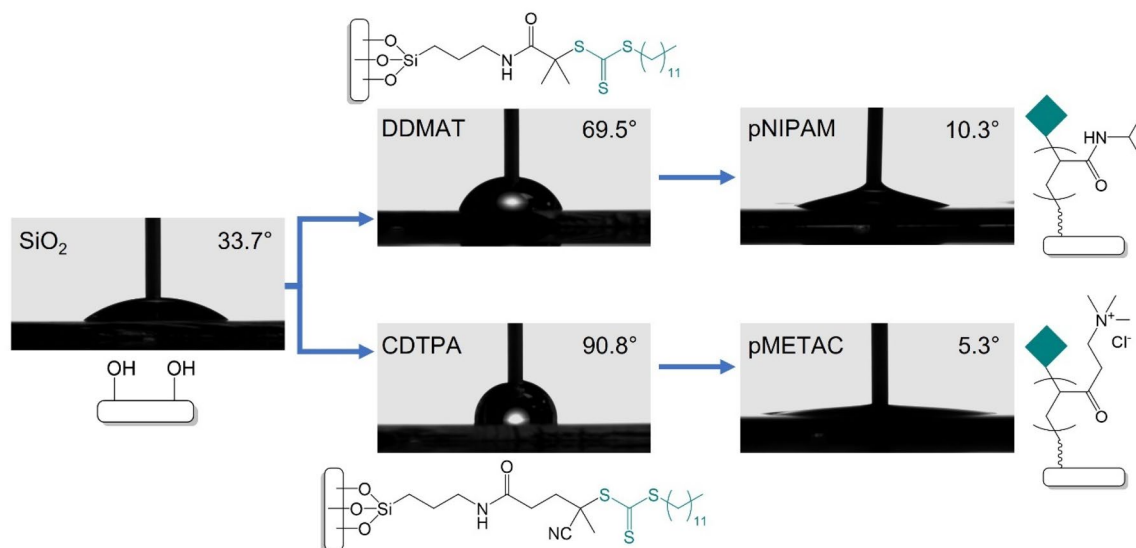


FIGURE 3 | Representative images of sessile droplets with embedded needle on unmodified, RAFT agent-functionalised, and polymer brush-decorated silicon wafers with their respective static contact angle values and schematic surface functional group representations. The pNIPAM and the pMETAC samples were both grafted under $\lambda = 405$ nm illumination.

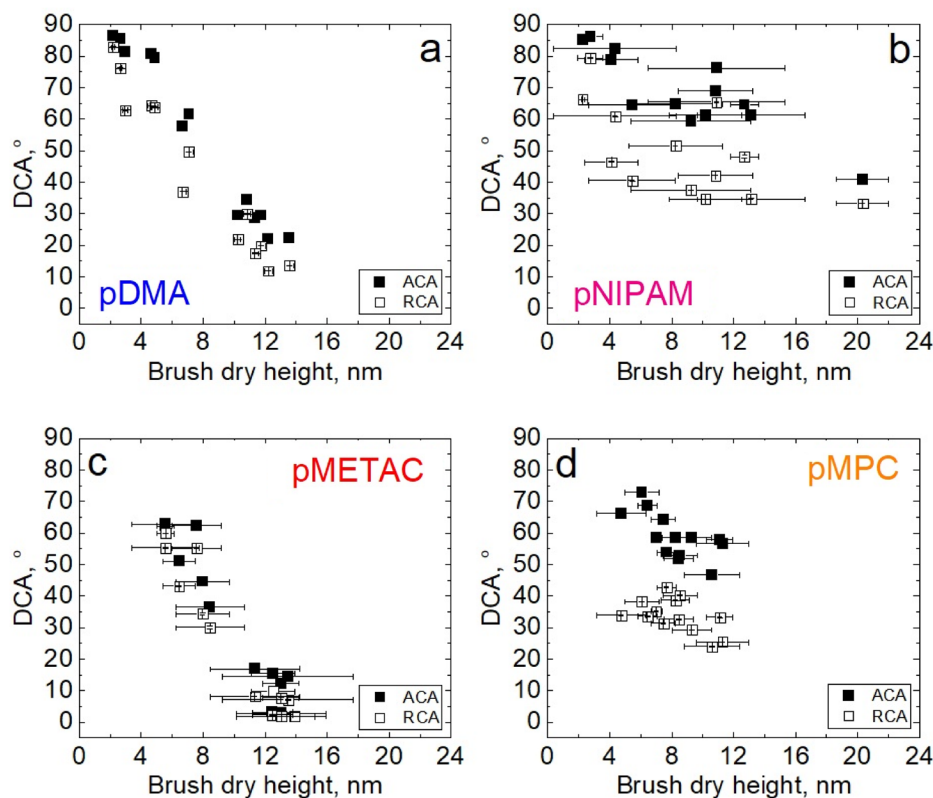


FIGURE 4 | DCA as a function of dry brush height of (a) pDMA, (b) pNIPAM, (c) pMETAC, and (d) pMPC brushes. Error bars indicate standard deviations of multiple measurements.

In our experiments, the achieved brush height was dependent on the irradiation wavelength, and as a result of this, the achieved wettability could be—although, only indirectly—also correlated with the irradiation wavelength: local minima in DCA (maxima in hydrophilicity) were observed as a result of the application of wavelengths around 405, 590, or 660 nm, matching the local extremities in brush height (Figure 2). Besides these

extremities, considering the relation between dry height and DCA (Figure 3), the other contact angle values also confirm the experienced wavelength-dependent height trends (Figure S10). These findings imply that dynamic contact angle experiments can complement or may even replace height measurements for polymer brush growth-related photochemical effects, for some monomer types.

3 | Conclusion

In this current work, we demonstrated that the growth in polymer brush height by SI-PET-RAFT significantly depends on the irradiation wavelength. We show that while the absorption maxima of the photocatalyst used, ZnTPPS₄⁴⁻, is in blue region (ca. 425 nm), the greatest brush heights obtained was in the lower absorption regions, mostly red-shifted. We found that the brush height was also dependent on the type of monomer used. To our knowledge, this photochemical action methodology has not been used previously on surveying maximum brush heights using the photoredox catalyst, ZnTPPS₄⁴⁻ over a broad range of wavelengths (from 375 to 700 nm). As the hydrophilicity of the brush-grafted surfaces generally showed increasing tendencies with increasing brush dry thickness, comparison of dynamic contact angles could also mean an alternative to ellipsometry in investigating the action plot characteristics. The use of lower energy wavelengths is an important step in the application of such photoinduced living polymerization technology for green up-scaled processes, which our results may better inform the SI-PET-RAFT brush community.

4 | Experimental Section/Methods

4.1 | Materials

[2-(Methacryloyloxy)ethyl]trimethylammonium chloride solution, 75 wt. % in H₂O (METAC), 2-methacryloyloxyethyl phosphorocholine (MPC), *N*-isopropylacrylamide (NIPAM), 2-(dodecylthio-carbonothioylthio)-2 methylpropionic acid (DDMAT), cyano-4-[(dodecylsulfanylthiocarbonyl)sulfanyl]pentanoic acid (CDTPA), (3-aminopropyl)triethoxysilane (APTES), *N*-(3-(dimethylamino)propyl)-*N'*-ethylcarbodiimide hydrochloride (EDC HCl) were purchased from Sigma-Aldrich and used as received (unless otherwise noted). Dichloromethane (DCM), toluene, isopropyl alcohol, ethyl acetate, and hexanes were purchased from Fisher Scientific and used as received. *N,N*-Dimethylacrylamide (DMA) was purified by passing through a short aluminum oxide column before the reaction. Zn(II) meso-tetra(4-sulfonatophenyl)-porphyrin (ZnTPPS₄⁴⁻) was obtained from Frontier Scientific and used as received. High-purity water (MilliQ water) with a resistivity of > 18.2 MΩ cm was obtained from an inline Millipore RiOs/Origin water purification system (Millipore Corporation, Massachusetts, USA). Polished single-crystal (100)-silicon wafers were obtained from Silicon Materials, Kaufering, Germany, with a native SiO₂ layer thickness of ~1.4 nm. Thorlabs Olympus M series mounted light-emitting diodes (LEDs) (λ_{max} = 365, 405, 455, 490, 530, 565, 590, 595, 617, 625, 660, 680, and 700 nm) were used for all light-mediated reactions. LED light intensities were modulated by a Thorlabs LED DC4100 4-channel LED driver. In terms of emission wavelength, all the applied LEDs have a ~50 nm wide emission regime, centered around the nominal, highest intensity emission wavelength. The spectra are available on the website of the manufacturer (Figure S2) [51].

4.2 | Instrumentation

The ¹H (500.13 MHz) NMR spectra were recorded using an AVANCE III 500 Spectrometer (Bruker, Germany) using CDCl₃ at 30°C. All ¹H NMR experiments are reported in δ units, parts per million (ppm), and were normalized to the signal for the

deuterated solvent CDCl₃ (7.26 ppm). Film thicknesses were measured by using a J.A. Woollam RC2-D variable-angle spectroscopic ellipsometer (VASE) at 70° incident angle and a wavelength range from 450 to 900 nm. The CompleteEASE software package (J.A. Woollam Co. Inc.) was used for fitting the optical constants and thicknesses. Unless otherwise noted, a three-layer model containing (a) a silicon substrate layer at the bottom, followed by (b) a 1.4 nm thick native silicon oxide layer and then (c) a polymer film layer were used. Thicknesses of polymer film layers were fitted by using a general Cauchy model. The UV-Vis absorbance spectra of the RAFT CTA solutions (2.74 mM in toluene) were recorded using a SPECORD 40 spectrophotometer (Analytik Jena, Jena, Germany).

4.3 | Synthesis of DDMAT and CDTPA Surface Initiators

DDMAT and CDTPA surface initiators were synthesized according to established procedures and characterized via ¹H NMR spectroscopy. DDMAT surface initiator: ¹H NMR (500 MHz, CDCl₃, 30°C, δ, ppm): 0.54 (s, 2H), 0.81 (t, 3H), 1.19 (t, 9H), 1.31 (m, 18H), 1.53 (m, 2H), 1.58 (m, 2H), 1.62 (s, 6H), 3.15 (q, 2H), 3.20 (t, 2H), 3.75 (q, 6H), 6.54 (t, 1H); CDTPA surface initiator: ¹H NMR (500 MHz, CDCl₃, 30°C, δ, ppm): 0.63 (s, 2H), 0.88 (t, 3H), 1.26 (t, 9H), 1.38 (m, 16H), 1.66 (m, 6H), 1.91 (s, 3H), 2.45 (m, 4H), 3.29 (t, 4H), 3.83 (q, 6H), 5.88 (t, 1H).

4.4 | General Preparation of Polymer Brushes Using SI-PET-RAFT

Silicon wafer substrates with a layer of native oxide were cut into 1 cm × 2 cm, cleaned by sonication in ethanol (three times), and then dried under a stream of nitrogen gas. The wafers were cleaned and activated by a plasma cleaner for around 1 min. After cleaning, the wafers were placed in a dilute solution containing 20 μL of synthesized DDMAT/CDTPA CTA in 40 mL of dry toluene, overnight at room temperature. After 24 h, the functionalised substrates were rinsed thoroughly with toluene followed by isopropanol and dried under a stream of nitrogen gas. These substrates were then subjected to polymerization. Unless otherwise noted, all reactions were placed approximately 13 cm below an LED light source (adjusted by the help of a so as the radiant flux was 1.82 mW cm⁻²). A stock solution containing 1 mg of photocatalyst (ZnTPPS₄⁴⁻) in 1 mL MilliQ was prepared in a vial and stored in the dark. DMA was purified through a basic alumina column to remove the inhibitor before use while NIPAM was re-crystallized with hexane. All liquid monomers (METAC or DMA), ascorbic acid (AA), and the ZnTPPS₄⁴⁻/MilliQ stock pre-polymerization solution were mixed with a molar ratio of [monomer]:[ascorbic acid]:[ZnTPPS₄⁴⁻] = 500:2:0.025, while for solids, that is, NIPAM and MPC, ratio used was [monomer]:[ascorbic acid]:[ZnTPPS₄⁴⁻] = 500:2:0.05, respectively [15].

A CTA-functionalised native oxide silicon wafer substrate was placed on top of a glass base plate. Then, 90 μL of the pre-polymerization reaction mixture containing METAC (2.84 mL) or DMA (2.92 mL) or MPC (2.2 g) with 10.8 mg AA in 1 mL ZnTPPS₄⁴⁻/MilliQ stock was dropped onto the substrate. NIPAM

(0.867 g) stock solution was prepared with 10.8 mg AA in 1:1 (MeOH:MilliQ) solution due to its insolubility in pure MilliQ. Furthermore, a glass coverslip was placed on top of the substrate to form a thin solution layer. Each sample was irradiated at a varied wavelength at a constant light intensity of 1.82 mW cm^{-2} , for 10 min except for METAC where polymerization was performed for 20 min. The irradiation was measured using a Thorlabs PM100D-Compact Power and Energy Meter Console. After irradiation, the substrates were thoroughly rinsed with DIW followed by isopropyl alcohol, and then dried under a nitrogen stream.

To confirm the negligible effect of RAFT CTA iniferter activity over brush height, DMA brushes were also synthesized excluding ZnTPPS_4^{4-} photocatalyst from the reaction mixture.

4.5 | Wettability

The DCAs were determined at room temperature, applying the embedded needle method [52, 53], using a DataPhysics OCA 40 drop contour analyzer and SCA 20 software (DataPhysics Instruments GmbH, Filderstadt, Germany). After de-dusting by nitrogen blowing, a MQ water droplet with $5 \mu\text{L}$ initial volume was deposited on the samples. By the help of the embedded steel needle ($d = 0.5 \text{ mm}$) of the dosing syringe, another $5 \mu\text{L}$ was added to the initial droplet, followed by the draining of the same volume, both at the same rate ($0.25 \mu\text{L s}^{-1}$), while a video of the droplet was recorded. The DCAs were obtained on the basis of tangential fitting to the drop contour in video frames. The averaged maximum and minimum plateau values of the obtained contact angle (Θ) versus time plots were denoted as advancing (Θ_A) and receding (Θ_R) contact angles, respectively. DCAs on each sample was measured in two different spots, while three samples (two in the case of $\lambda = 365 \text{ nm}$) were analyzed for each monomer-illumination wavelength combination, resulting in at least four DCA pairs for each set of sample parameters.

The contact angle hysteresis (CAH) values were calculated according to Equation (1):

$$\text{CAH} = \text{ACA} - \text{RCA} \quad (1)$$

The representative static contact angles presented in Figure 3 were calculated on the basis of tangential fitting in the first frame of the respective DCA videos. The applied data processing procedure is described in the (Table S1).

Acknowledgments

The authors gratefully acknowledge the Deutsche Forschungsgemeinschaft (DFG) for funding project 496201730 ((BE 7737/2-1) (Q.A.B., K.R., L.M.)), and the Alexander von Humboldt Foundation (J.Y.). The first three authors (L.M., K.R., and J.Y.) contributed equally to this work. We gratefully acknowledge Dr. Eva Bittrich for assistance with in situ ellipsometry, and Prof. Christopher Barner-Kowollik for enlightening discussions.

References

1. Y. Higaki, M. Kobayashi, D. Murakami, and A. Takahara, "Anti-Fouling Behavior of Polymer Brush Immobilized Surfaces," *Polymer Journal* 48 (2016): 325–331.

2. G. C. Ritsema van Eck, L. Chiappisi, and S. de Beer, "Fundamentals and Applications of Polymer Brushes in Air," *ACS Applied Polymer Materials* 4 (2022): 3062–3087.
3. A. R. Kuzmyn, L. W. Teunissen, M. V. Kroese, J. Kant, S. Venema, and H. Zuilhof, "Antiviral Polymer Brushes by Visible-Light-Induced, Oxygen-Tolerant Covalent Surface Coating," *ACS Omega* 7 (2022): 38371–38379.
4. C. W. Pester, H.-A. Klok, and E. M. Benetti, "Opportunities, Challenges, and Pitfalls in Making, Characterizing, and Understanding Polymer Brushes," *Macromolecules* 56 (2023): 9915–9938.
5. Q. A. Besford, H. Merlitz, S. Schubotz, et al., "Mechanofluorescent Polymer Brush Surfaces That Spatially Resolve Surface Solvation," *ACS Nano* 16 (2022): 3383–3393.
6. Q. A. Besford, H. Yong, H. Merlitz, et al., "FRET-Integrated Polymer Brushes for Spatially Resolved Sensing of Changes in Polymer Conformation," *Angewandte Chemie International Edition* 60 (2021): 16600–16606.
7. Q. A. Besford, S. Schubotz, S. Chae, et al., "Molecular Transport Within Polymer Brushes: A FRET View at Aqueous Interfaces," *Molecules* 27, no. 9 (2022): 3043, <https://doi.org/10.3390/molecules27093043>.
8. Q. A. Besford, P. Uhlmann, and A. Fery, "Spatially Resolving Polymer Brush Conformation: Opportunities Ahead," *Macromolecular Chemistry and Physics* 224, no. 1 (2023): 2200180, <https://doi.org/10.1002/macp.202200180>.
9. A. Murad Bhayo, Y. Yang, and X. He, "Polymer Brushes: Synthesis, Characterization, Properties and Applications," *Progress in Materials Science* 130 (2022): 101000, <https://doi.org/10.1016/j.pmatsci.2022.101000>.
10. A. M. Jazani, H. Murata, M. Cvek, et al., "Aqueous Photo-RAFT Polymerization Under Ambient Conditions: Synthesis of Protein-Polymer Hybrids in Open Air," *Chemical Science* 15 (2024): 9742–9755.
11. D. Lee, H. Wang, and R. Verdusco, "Development of an Open-Source Methodology for Simulation of Civil Engineering Structures Subject to Multi-Hazards," *Journal of Polymer Science* 62 (2024): 3879–3896.
12. M. L. Allegranza and D. Konkolewicz, "PET-RAFT Polymerization: Mechanistic Perspectives for Future Materials," *ACS Macro Letters* 10 (2021): 433–446.
13. Y. Lee, C. Boyer, and M. S. Kwon, "Photocontrolled RAFT Polymerization: Past, Present, and Future," *Chemical Society Reviews* 52 (2023): 3035–3097.
14. S. Shanmugam, J. Xu, and C. Boyer, "Exploiting Metalloporphyrins for Selective Living Radical Polymerization Tunable Over Visible Wavelengths," *Journal of the American Chemical Society* 137 (2015): 9174–9185.
15. M. Li, M. Fromel, D. Ranaweera, S. Rocha, C. Boyer, and C. W. Pester, "SI-PET-RAFT: Surface-Initiated Photoinduced Electron Transfer-Reversible Addition-Fragmentation Chain Transfer Polymerization," *ACS Macro Letters* 8 (2019): 374–380.
16. J. Poisson, A. M. Polgar, M. Fromel, C. W. Pester, and Z. M. Hudson, "Preparation of Patterned and Multilayer Thin Films for Organic Electronics via Oxygen-Tolerant SI-PET-RAFT," *Angewandte Chemie International Edition* 60 (2021): 19988–19996.
17. X. Xu, X. Huang, Y. Chang, et al., "Antifouling Surfaces Enabled by Surface Grafting of highly Hydrophilic Sulfoxide Polymer Brushes," *Biomacromolecules* 22 (2021): 330–339.
18. G. Ng, M. Li, J. Yeow, K. Jung, C. W. Pester, and C. Boyer, "Benchmark Preparation of Polymer Brushes by SI-PET-RAFT: The Effect of the Polymer Composition and Structure on Inhibition of a Pseudomonas Biofilm," *ACS Applied Materials & Interfaces* 12 (2020): 55243–55254.
19. S. Shanmugam, J. Xu, and C. Boyer, "Aqueous RAFT Photopolymerization With Oxygen Tolerance," *Macromolecules* 49 (2016): 9345–9357.

20. M. Fromel, D. M. Sweeder, S. Jang, T. A. Williams, S. H. Kim, and C. W. Pester, "Superhydrophilic Polymer Brushes With High Durability and Anti-Fogging Activity," *ACS Applied Polymer Materials* 3 (2021): 5291–5301.
21. J. Xu, S. Shanmugam, H. T. Duong, and C. Boyer, "Organo-Photocatalysts for Photoinduced Electron Transfer-Reversible Addition–Fragmentation Chain Transfer (PET-RAFT) Polymerization," *Polymer Chemistry* 6 (2015): 5615–5624.
22. B. Nomeir, O. Fabre, and K. Ferji, "Organo-Photocatalysts for Photoinduced Electron Transfer-Reversible Addition–Fragmentation Chain Transfer (PET-RAFT) Polymerization," *Macromolecules* 52 (2019): 6898–6903.
23. A. Bagheri, C. W. A. Bainbridge, K. E. Engel, et al., "Oxygen Tolerant PET-RAFT Facilitated 3D Printing of Polymeric Materials Under Visible LEDs," *ACS Applied Polymer Materials* 2 (2020): 782–790.
24. E. Roeven, A. R. Kuzmyn, L. Scheres, J. Baggerman, M. M. J. Smulders, and H. Zuilhof, "PLL–Poly(HPMA) Bottlebrush-Based Antifouling Coatings: Three Grafting Routes," *Langmuir* 36 (2020): 10187–10199.
25. A. R. Kuzmyn, M. Van Galen, B. Van Lagen, and H. Zuilhof, "SI-PET-RAFT in Flow: Improved Control Over Polymer Brush Growth," *Polymer Chemistry* 14 (2023): 3357–3363.
26. S. L. Walden, J. A. Carroll, A. N. Unterreiner, and C. Barner-Kowollik, "Photochemical Action Plots Reveal the Fundamental Mismatch Between Absorptivity and Photochemical Reactivity," *Advanced Science* 11 (2024): 11.
27. N. M. Barbosa Neto, S. L. Oliveira, L. Misoguti, et al., "Singlet Excited State Absorption of Porphyrin Molecules for Pico- and Femtosecond Optical Limiting Application," *Journal of Applied Physics* 99, no. 12 (2006): 123103, <https://doi.org/10.1063/1.2204350>.
28. K. Anjali, L. K. Nishana, J. Christopher, and A. Sakthivel, "Zinc-Tetraphenylporphyrin Grafted on Functionalised Mesoporous SBA-15: Synthesis and Utilisation for Nitroaldol Condensation," *Journal of Porous Materials* 27 (2020): 1191–1201.
29. P. J. Gonçalves, L. De Boni, I. E. Borissevitch, and S. C. Zílio, "Excited State Dynamics of Meso-Tetra(Sulphonatophenyl) Metalloporphyrins," *Journal of Physical Chemistry A* 112 (2008): 6522–6526.
30. J. Xu, S. Shanmugam, C. Fu, K.-F. Aguey-Zinsou, and C. Boyer, "Excited State Dynamics of Meso-Tetra(Sulphonatophenyl) Metalloporphyrins," *Journal of the American Chemical Society* 138 (2016): 3094–3106.
31. S. C. Gauci, F. E. Du Prez, J. O. Holloway, H. A. Houck, and C. Barner-Kowollik, "The Power of Action Plots: Unveiling Reaction Selectivity of Light-Stabilized Dynamic Covalent Chemistry," *Angewandte Chemie International Edition* 62 (2023): e202310274.
32. N. Corrigan, J. Yeow, P. Judzewitsch, J. Xu, and C. Boyer, "Seeing the Light: Advancing Materials Chemistry Through Photopolymerization," *Angewandte Chemie International Edition* 58 (2019): 5170–5189.
33. M. Hartlieb, "Photo-Initiated RAFT Polymerization," *Macromolecular Rapid Communications* 43 (2022): 2100514.
34. J. Luo, M. Li, M. Xin, W. Sun, and W. Xiao, "Visible Light Induced RAFT Polymerization of 2-Vinylpyridine without Exogenous Initiators or Photocatalysts," *Macromolecular Chemistry and Physics* 217 (2016): 1777–1784.
35. P. J. Gonçalves, I. E. Borissevitch, and S. C. Zílio, "Effect of Protonation on the Singlet–Singlet Excited-State Absorption of Meso-Tetrakis (p-sulphonatophenyl) Porphyrin," *Chemical Physics Letters* 469 (2009): 270–273.
36. J. Valančiūnaitė, J. Žerebcova, S. Bagdonas, G. Streckytė, and R. Rotomskis, "Spectroscopic Studies of Self-Assembled TPPS 4 Nanostructures in Aqueous Solutions: The Role of Serum Albumin and pH," *Lithuanian Journal of Physics and Technical Sciences* 44, no. 1 (2004): 41–47, <https://doi.org/10.3952/lithjphys.44105>.
37. S. Shanmugam, J. Xu, and C. Boyer, "A Logic Gate for External Regulation of Photopolymerization," *Polymer Chemistry* 7 (2016): 6437–6449.
38. J. Mandal, R. Simic, and N. D. Spencer, "Tuning and In Situ Monitoring of Surface-Initiated, Atom-Transfer Radical Polymerization of Acrylamide Derivatives in Water-Based Solvents," *Polymer Chemistry* 10, no. 29 (2019): 3933–3942, <https://doi.org/10.1039/C9PY00587K>.
39. M. H. Futscher, M. Philipp, P. Müller-Buschbaum, and A. Schulte, "The Role of Backbone Hydration of Poly(N-Isopropyl Acrylamide) Across the Volume Phase Transition Compared to Its Monomer," *Scientific Reports* 7, no. 1 (2017): 17012, <https://doi.org/10.1038/s41598-017-17272-7>.
40. G. Aktas Eken and C. K. Ober, "Strong Polyelectrolyte Brushes via Alternating Copolymers of Styrene and Maleimides: Synthesis, Properties, and Stability," *Macromolecules* 55 (2022): 5291–5300.
41. M. Fromel and C. W. Pester, "Polycarbonate Surface Modification via Aqueous SI-PET-RAFT," *Macromolecules* 55 (2022): 4907–4915.
42. P. Muller, G. Sudre, and O. Théodoly, "Wetting Transition on Hydrophobic Surfaces Covered by Polyelectrolyte Brushes," *Langmuir* 24 (2008): 9541–9550.
43. K. C. Bentz and D. A. Savin, "Chain Dispersity Effects on Brush Properties of Surface-Grafted Polycaprolactone-Modified Silica Nanoparticles: Unique Scaling Behavior in the Concentrated Polymer Brush Regime," *Macromolecules* 50 (2017): 5565–5573.
44. J. C. Conrad and M. L. Robertson, "Shaping the Structure and Response of Surface-Grafted Polymer Brushes via the Molecular Weight Distribution," *JACS Au* 3 (2023): 333–343.
45. K. Grundke, K. Pöschel, A. Synytska, et al., "Experimental Studies of Contact Angle Hysteresis Phenomena on Polymer Surfaces – Toward the Understanding and Control of Wettability for Different Applications," *Advances in Colloid and Interface Science* 222 (2015): 350–376.
46. C. N. C. Lam, N. Kim, D. Hui, D. Y. Kwok, M. L. Hair, and A. W. Neumann, "The effect of Liquid Properties to Contact Angle Hysteresis," *Colloids and Surfaces A: Physicochemical and Engineering Aspects* 189 (2001): 265–278.
47. W. Feng, J. Brash, and S. Zhu, "Atom-Transfer Radical Grafting polymerization of 2-Methacryloyloxyethyl Phosphorylcholine From Silicon Wafer Surfaces," *Journal of Polymer Science Part A: Polymer Chemistry* 42 (2004): 2931–2942.
48. K. N. Plunkett, X. Zhu, J. S. Moore, and D. E. Leckband, "PNIPAM Chain Collapse Depends on the Molecular Weight and Grafting Density," *Langmuir* 22 (2006): 4259–4266.
49. W. Yang, R. Zhang, Y. Wu, et al., "Enhancement of Graft Density and Chain Length of Hydrophilic Polymer Brush for Effective Marine Antifouling," *Journal of Applied Polymer Science* 135, no. 22 (2018): 46232, <https://doi.org/10.1002/app.46232>.
50. N. Cheng, A. A. Brown, O. Azzaroni, and W. T. S. Huck, "Thickness-Dependent Properties of Polyzwitterionic Brushes," *Macromolecules* 41 (2008): 6317–6321.
51. "Thorlabs, Mounted LED Product Descriptions," 2024, https://www.thorlabs.de/newgrouppage9.cfm?objectgroup_id=2692.
52. J. Drelich, "Guidelines to Measurements of Reproducible Contact Angles Using a Sessile-Drop Technique," *Surface Innovations* 1 (2013): 248–254.
53. A. Kormányos, B. Endrődi, Z. Zhang, et al., "Local Hydrophobicity Allows High-Performance Electrochemical Carbon Monoxide Reduction to C²⁺ Products," *EES Catalysis* 1 (2023): 263–273.

Supporting Information

Additional supporting information can be found online in the Supporting Information section.